Technical Sciences
Academy of Romania
www.jesi.astr.ro

Journal of Engineering Sciences and Innovation
Volume 8, Issue 3 / 2023, pp. 251-268
http://doi.org/10.56958/jesi.2023.8.3.251

D. Environmental Engineering and Energy

Received ***14 Apryl 2023*** *Accepted* ***27 September 2023***
Received in revised form ***21 July 2023***

Best operation strategies for piezoelectric vibration energy harvesters. II. Application to simple or induction-assisted resistive loads

VIOREL BADESCU[*]

Candida Oancea Institute, Polytechnic University of Bucharest, Spl. Independentei 313, Bucharest 060042, Romania

Abstract. The controllable load consists of a resistive load (with two types of controls, i.e. a controllable resistance and a controllable inductance). Generally, the optimal control of the resistance near the resonance value is of bang-bang type and the harvested energy increases by increasing the variation range of the controllable resistance. Also, in case the controllable resistance is significantly smaller than the resonance value, the harvested energy increases by increasing the upper bound of the allowed interval of resistance variation. Users who need small amounts of energy might be interested in the utilization of a single cycle of the vibration energy source. Several energy sources have been considered and the harvested power for the first cycle ranges between about 10^{-20} and 10^{-8} W.

Keywords: piezoelectric energy harvester; direct optimal control; resistance load.

1. Introduction

In this paper we focus on piezoelectric energy harvesters whose electrical load consists of a variable resistor whose operation is optimally controlled. The theory has been proposed in part I of the paper [1]. Achieving high effectiveness of the energy harvesting devices is subjected usually to strong inherent and practical constraints such as displacement [2] or transduction mechanisms constraints [3]. Constrained optimal control is used here but the constraints are acting on load characteristics.

[*]Correspondence address: badescu@theta.termo.pub.ro

2. Resistive load

Several ferroelectric materials have good piezoelectric properties. They include perovskite-type piezoceramics such as PZT (lead zirconium titanate) and BaTiO3 barium titanate) as well as ZnO (zinc oxide), which has, however, relatively little piezoelectric oupling [4]. Sputtered $KNbO_3$ nanocoatings for flexible energy harvesting have been also tested [5]. Several materials including BaTiO3, PbTiO3, PbZrTiO3, PZT-5A and PZT-5H piezoelectric crystals have been experimented for energy recovery from induced mechanical vibration in vehicle suspension [6]. The material PZT-5H is considered here. Comparisons with results obtained for other material (PZT-5A) are shown in the Electronic Supplementary Material (ESM).
Further information about the system may be found in [4] including design details which are shortly presented in Table 1. These values are used in this work. Exceptions are clearly specified when needed.

Table 1. Main characteristics of the system treated here.

Piezoelectric material properties (PZT-5H)	
Stiffness coefficient (in short circuit conditions), c_{33}^E	$48.3\cdot 10^9\ N/m^2$
Piezoelectric constant, e_{33}	$28.64\,C/m^2$
Permittivity of the piezoelectric element, ε_{33}^S	$1.317\cdot 10^{-8}\ F/m$
Design quantities	
Cross sectional surface area through the piezoelectric element, A_p	$10^{-4}\ m^2$
Thickness of un-deformed piezoelectric element, t_p	$10^{-2}\ m$
Proof mass, M	$0.01\,kg$
Mass of piezoelectric element, m_p	$0.0075\,kg$
Mechanical damping ratio, ζ_m	0.05
Characteristics of the vibratory energy source (the base excitation)	
Frequency, $f=\frac{\omega}{2\pi}$	$120\ Hz$
Magnitude of acceleration, a	$1.276\,m/s^2$

Values quite similar with those of Table 1 are used in [7] where a lower acceleration value is adopted. Notice that the properties of the known piezoelectric materials deviate from non-resonant values at material resonance. However, the linear behavior of the transducer over all frequencies is assumed by most researchers [4] and this approximation is adopted here.

Most previous optimal control approaches where the load consists of a resistance assume that resistance is among the controls. This case is considered here. However, another case with resistive load is also treated in paper [8] where the power is maximized by using a controllable inductor. Notice that both the resistance and the inductance were optimized in [7] but a operation at classical resonance assumption was adopted there.

2.1. Usage of load resistance as a control

The scheme shown in Fig. 1a is used in the following. The harvesting circuit is generically described by a series resistor of resistance R_{hs} and a parallel resistor of resistance R_{hp} (which may include the parallel resistance of the piezoelectric element). This is in concordance with [9] where the power losses in the electronic circuit are assumed quadratic and purely resistive. The load is described by a resistor of resistance R_l. The electric current through the parallel resistor is denoted i_{Rhp} while the current trough the load resistor is denoted i_h.

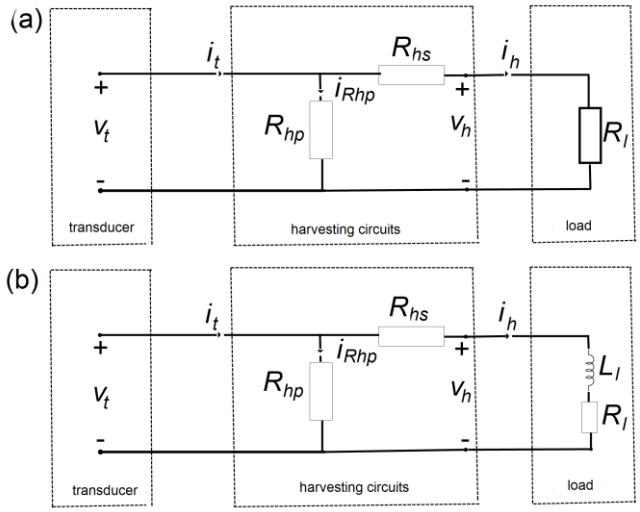

Fig. 1. Particular scheme of a controlled vibration energy harvesting system. (a) load resistance is used as a control; (b) the inductance of the load is used as a control.

The voltage v_h across the load resistor is given by:

$$v_h = v_t - i_h R_{hs} \tag{1}$$

The usage of the Kirchoff's law for nodes yields:

$$i_t = i_{Rhp} + i_h \tag{2}$$

By definition, the current generated by the piezoelectric element equals the time variation of its electrical charge:

$$i_t \equiv \dot{q}_t \tag{3}$$

where the dot means time derivative. This is the usual approach [10]. Usage of the Ohm law and Eq. (1) yield:

$$i_{Rhp} = \frac{v_t}{R_{hp}} \tag{4}$$

while the usage of the Kirchoff's law for circuits yields:

$$v_t = i_h\left(R_{hs} + R_l\right) \tag{5}$$

Usage of Eqs. (14) and (15) of [1] gives:

$$\ddot{z} + 2\zeta_m \omega_N \dot{z} + \omega_N^2 z + \frac{\theta}{M_T}\left(\frac{q_t + \theta z}{C_p}\right) = -\ddot{w}_B \tag{6}$$

The four terms in the l.h.s of Eq. (6) are related with the kinetic energy, the mechanical losses, the elastic energy and the harvested energy, respectively. The usage of Eqs. (2), (3), (4), (5) and Eq. (15) of [1] yield:

$$\dot{q}_t = -\frac{q_t + \theta z}{C_p}\left(\frac{1}{R_{hp}} + \frac{1}{R_{hs} + R_l}\right) \tag{7}$$

Notice that the product $R_l C_p$ is the time constant of the electrical circuit [4].

Equations (6) and (7) constitute a system of two equations with two unknown, i.e. z and q_t. These equations are solved with the following initial conditions:

$$z\left(\tau = 0\right) = 0 \tag{8}$$

$$q_t\left(\tau = 0\right) = 0 \tag{9}$$

which means that the piezoelectric element is not deformed in the initial state.

Different cost functions are defined for power harvesting and power dissipation [11]. Here the objective function is the electric energy $E_{l,T}$ dissipated as heat on the load resistor during the time interval T is:

$$E_{l,T} = \int_0^T R_l i_h^2 d\tau = \int_0^T R_l \left(\frac{q_t + \theta z}{C_p\left(R_{hs} + R_l\right)}\right)^2 d\tau \qquad \text{(10a,b)}$$

Equation (15) of [1] and Eq. (5) have been used in Eq. (10b).

The objective is to maximize the electric energy $E_{l,T}$ by using a time variable resistance R_l, which is used as a control. This objective is almost similar with the cost function of [3] where an average output power is considered. Some previous optimal control studies where the control is load resistance define the objective function in a way similar with Eq. (10a) with T being the period of input harmonic vibration [11,3]. Here the integration time interval in Eqs. (10a, b) is not specified. In some papers the condition of periodic steady-state operation is imposed [11]. This requires modulation of the electromagnetic damping coefficient. If this is not the case, the operation is not periodic and differences exist between the output energy during several subsequent cycles, as will be shown in the following.

The optimal control problem defined by the objective function Eq. (10b) and the constraints Eqs. (6) and (7) constitutes a Bolza problem, which may be transformed into a Mayer problem in two steps. First, a new dependent variable E_l is defined by using the following equation:

$$\frac{dE_l}{d\tau} = R_l\left(\frac{q_t + \theta z}{C_p\left(R_{hs} + R_l\right)}\right)^2 \tag{11}$$

with the boundary (initial) condition:

$$E_l\left(\tau = 0\right) = 0 \tag{12}$$

Second, a new form of the objective, associated with the Mayer problem, is defined:

$$E_l\left(\tau = T\right) \rightarrow max \tag{13}$$

Table 2 shows the dimensionless notation, the coefficients and the equations for a system where the load consists of a resistor with controllable resistance.

Table 2. Dimensionless notation, coefficients and equations for the load consisting of a resistor with controllable resistance

Notation

$\hat{\tau} \equiv \frac{\tau}{\tau_{ref}}$ $\quad \hat{R}_l \equiv \frac{R_l}{R_{l,ref}}$ $\quad \hat{R}_{hp} \equiv \frac{R_{hp}}{R_{l,ref}}$ $\quad \hat{R}_{hs} \equiv \frac{R_{hs}}{R_{l,ref}}$

$\hat{h}_1 \equiv \frac{z}{z_{ref}}$ $\quad \hat{h}_2 \equiv \frac{\dot{z}}{\dot{z}_{ref}}$ $\quad \hat{h}_3 \equiv \frac{q_t}{q_{t,ref}}$ $\quad \hat{h}_4 \equiv \frac{E}{E_{ref}}$

Coefficients

$A_{12} \equiv \frac{\dot{z}_{ref}\tau_{ref}}{z_{ref}}$

$A_{21} \equiv -\left(\omega_N^2 + \frac{\theta^2}{M_T C_p}\right)\frac{z_{ref}\tau_{ref}}{\dot{z}_{ref}}$ $\quad A_{22} \equiv -2\zeta_m\omega_N\tau_{ref}$ $A_{23} \equiv -\frac{\theta}{M_T C_p}\frac{q_{t,ref}\tau_{ref}}{\dot{z}_{ref}}$ $\quad A_{2w} \equiv -\frac{a\tau_{ref}}{\dot{z}_{ref}}$

$A_{31} \equiv -\frac{\theta}{C_p}\frac{z_{ref}\tau_{ref}}{q_{t,ref}R_{l,ref}}$ $\quad A_{33} \equiv -\frac{\tau_{ref}}{R_{l,ref}C_p}$ $\quad B_{2w} \equiv 2\pi f\tau_{ref}$

$A_{41} \equiv \frac{\theta^2 z_{ref}^2\tau_{ref}}{E_{ref}R_{l,ref}C_p^2}$ $\quad A_{43} \equiv \frac{q_{t,ref}^2\tau_{ref}}{E_{ref}R_{l,ref}C_p^2}$ $A_{413} \equiv \frac{2\theta z_{ref}q_{t,ref}\tau_{ref}}{E_{ref}R_{l,ref}C_p^2}$

Equations

$\frac{d\hat{h}_1}{d\hat{\tau}} = A_{12}\hat{h}_2$

$$\frac{d\hat{h}_2}{d\hat{\tau}} = A_{21}\hat{h}_1 + A_{22}\hat{h}_2 + A_{23}\hat{h}_3 + A_{2w}\cos\left(B_{2w}\hat{\tau}\right)$$

$$\frac{d\hat{h}_3}{d\hat{\tau}} = \left(\frac{1}{\hat{R}_{hp}} + \frac{1}{\hat{R}_{hs} + \hat{R}_l}\right)\left(A_{31}\hat{h}_1 + A_{33}\hat{h}_3\right)$$

$$\frac{d\hat{h}_4}{d\hat{\tau}} = \frac{1}{\hat{R}_l}\left(A_{41}\hat{h}_1^2 + A_{43}\hat{h}_3^2 + A_{413}\hat{h}_1\hat{h}_3\right)$$

Initial conditions

$$\hat{h}_i\left(\hat{\tau} = 0\right) = 0 \quad \left(i = 1{,}4\right)$$

Several assumptions have to be made in order to make the mathematical problem more tractable, including that the state and control functions are measurable, the displacement is absolutely continuous and the equations are satisfied for all time moments except a set of null measure [11]. Passive controller is assumed here since the net energy injection during controller operation is neglected [3]. Also, conservative (lossless) controller is assumed, as adopted in [3]. Achieving high effectiveness of the energy harvesting devices is subjected usually to strong inherent and practical constraints such as displacement or transduction mechanisms constraints [3]. Since small displacements are considered, no constraint is assumed here for the displacement. An example of constrained displacement may be found in [3]. The optimal load and stiffness of a harmonically driven two-port harvester with displacement constraints has been determined analytically in [12]. MEMS electrostatic energy harvesters with end-stop effects have been treated in [13,14]. However, constraints have been considered here for the controlled resistance of the load.

2.1.1. Results

The vibratory energy resource has quasi-periodic characteristics. Here we make the assumption that it consists of similar cycles and a number of ten cycles is considered. In terms of the dimensionless time this means that the final time is $\hat{\tau}_f = 1$ and $\tau_{ref} = 0.08333\,s$. The follow reference values have used in BOCOP to obtain dimensionless quantities: $h_{1,ref} = 10^{-11}$, $h_{2,ref} = 10^{-2}$, $h_{3,ref} = 10^{-10}$, $h_{4,ref} = 10^{-12}$.

In many previous studies dealing with energy harvesting systems the systems of ODEs have constant coefficients. This allows using classical solution procedures such as that based on Laplace transform, which has been widely used [15],[4],[16],[17]. However, optimal control approaches yield highly stiff ODEs with time-dependent coefficients and this requires usage of numerical solution procedures. The high drive frequency yields highly stiff ODEs and, as a consequence, suitable numerical procedures with small enough time step size

should be used. For instance, the dimensionless time step in [18] is lower than 10^{-5} to avoid stability problems of the numerical solution and the discretization of the controls is made with time step of $2 \cdot 10^{-5}$.

Several optimization methods are available in BOCOP and the Midpoint method is recommended and used here. A tolerance value $tol = 10^{-18}$ is adopted during numerical resolution.

The accuracy of the solution depends on the finesse of the discretization, which is described by the number n_{steps} of steps to divide the interval $\left[0, \hat{t}_f\right]$. We have performed several tests in order to find the most suitable number of steps. A constant value have been adopted for the control $\hat{R}_l$. In this case the optimization problem reduces to an usual initial value problem which consists of solving the four ordinary differential equations in Table 2 under the initial values in that Table 2. This has been performed by using an accurate solver (DDRIV3)[19]). The following values have been used for the parameters of this solver: EPS = 10^{-6}, HMAX=10^{-6}, EWT = 10^{-6}. The results obtained by using DDRIV3 solver are used as a reference. A similar procedure has been use during the optimal control approach adopted in [18]. Simulations were performed with fixed control values by using LT-SPICE software and the results are used as reference solutions

Previous results obtained by using indirect optimal control methods show that the optimal strategy consists of regular and singular phases [11]. The first case means the control is either at its minimum or at its maximum allowed value. This is also called bang-bang control [18]. The second case means the smooth time variation of the control. However, notice that in [11] a semi-active control technique is proposed since the controlled parameter is the damping electromagnetic coefficient which is modulated in time between a minimum and a maximum value and this is performed by appropriate change the resistance of the harvesting circuit. A different approach is adopted here since the control parameter is the load resistance.

Table 3 shows results obtained by using BOCOP and DDRIV3 solvers as a function of the number of steps n_{steps} for three constant values of the dimensionless load resistance $\hat{R}_l$. When the resonance load resistance is considered ($\hat{R}_l = 4.399$), BOCOP and DDRIV3 may be run on the available platforms only for numbers of steps lower that 15000 and this does not ensure convergence (BOCOP overestimates by about 20% the results provided by DDRIV3). However, when more realistic, far from resonance, load resistance values are considered, the results provided by BOCOP are in good agreement with those provided by DDRIV3 at large number of steps. The value $n_{steps} = 15000$ is adopted for next computations, as a compromise between better results accuracy and shorter computing time.

Table 3. Maximum energy per 10 cycles (in pJ) . Dependence on the number of steps n_{steps} for different solvers. Three constant values of $\hat{R}_l$ have been considered.

Constant value of $\hat{R}_l$		4.399		0.1
Solver	DDRIV3 (reference)	BOCOP (Midpoint)	DDRIV3 (reference)	BOCOP (Midpoint)
Number of steps				
1000	**5.2980**	4.0926	**0.2117**	0.4313
5000	**5.2991**	4.0912	**0.2118**	0.4104
10000	**5.3354**	4.0911	**0.4411**	0.4310
15000	**5.3351**	4.0911	**0.4334**	0.4310
20000			**0.4386**	
25000			**0.4382**	

Constant value of $\hat{R}_l$		0.004339
Solver	DDRIV3 (reference)	BOCOP (Midpoint)
Number of steps		
1000	**0.0163**	0.1653
5000	**0.0950**	0.1651
10000	**0.1673**	0.1651
15000	**0.1668**	0.1651
20000		
25000		

When the resistance R_{hs} is significantly smaller than R_l, the ordinary differential equations acting as constraints in Table 2 are quasi-linear in $1/\hat{R}_l$. Therefore, the control $\hat{R}_l$ is either constant or of the bang-bang type, i.e. it jumps between the smaller and the larger allowed values, $\hat{R}_{l,\min}$ and $\hat{R}_{l,\max}$, respectively.

Table 4 shows the maximum energy per 10 cycles for three constant values of $\hat{R}_{l,\,ref}$ and different couples of values $\hat{R}_{l,\min}$ and $\hat{R}_{l,\max}$.

Table 4. Maximum energy per 10 cycles (in pJ) . Three constant values of $\hat{R}_{l,\,ref}$ and different couples of values $\hat{R}_{l,\min}$ and $\hat{R}_{l,\max}$ have been considered. Midpoint method and $n_{steps} = 15000$.

$\hat{R}_{l,ref}$	$\hat{R}_{l,\min}$	$\hat{R}_{l,\max}$	Energy per 10 cycles (pJ)
4.399	$\hat{R}_{l,ref}$	$1.1\hat{R}_{l,ref}$	4.1906
	$\hat{R}_{l,ref}$	$1.2\hat{R}_{l,ref}$	4.2666
	$\hat{R}_{l,ref}$	$1.3\hat{R}_{l,ref}$	4.3476
	$\hat{R}_{l,ref}$	$\hat{R}_{l,ref}$	**4.0911**
	$0.9\hat{R}_{l,ref}$	$\hat{R}_{l,ref}$	4.2122
	$0.8\hat{R}_{l,ref}$	$\hat{R}_{l,ref}$	4.3369
	$0.7\hat{R}_{l,ref}$	$\hat{R}_{l,ref}$	4.4649
0.1	$\hat{R}_{l,ref}$	$1.1\hat{R}_{l,ref}$	0.4523
	$\hat{R}_{l,ref}$	$1.2\hat{R}_{l,ref}$	0.4736
	$\hat{R}_{l,ref}$	$1.3\hat{R}_{l,ref}$	0.4948
	$\hat{R}_{l,ref}$	$\hat{R}_{l,ref}$	**0.4310**
	$0.9\hat{R}_{l,ref}$	$\hat{R}_{l,ref}$	0.4334
	$0.8\hat{R}_{l,ref}$	$\hat{R}_{l,ref}$	0.4359
	$0.7\hat{R}_{l,ref}$	$\hat{R}_{l,ref}$	0.4385
0.004399	$\hat{R}_{l,ref}$	$1.1\hat{R}_{l,ref}$	0.1719
	$\hat{R}_{l,ref}$	$1.2\hat{R}_{l,ref}$	0.1780
	$\hat{R}_{l,ref}$	$1.3\hat{R}_{l,ref}$	0.1836
	$\hat{R}_{l,ref}$	$\hat{R}_{l,ref}$	**0.1651**
	$0.9\hat{R}_{l,ref}$	$\hat{R}_{l,ref}$	0.1651
	$0.8\hat{R}_{l,ref}$	$\hat{R}_{l,ref}$	0.1651
	$0.7\hat{R}_{l,ref}$	$\hat{R}_{l,ref}$	0.1651

In case of the large (resonance) reference value $\hat{R}_{l,ref} = 4.399$, the maximum energy for a constant load resistance $\hat{R}_l = \hat{R}_{l,ref}$ is smaller than the maximum energy harvested when the load resistance is allowed to vary in the interval $\left[\hat{R}_{l,\min}, \hat{R}_{l,\max}\right]$, either below or above $\hat{R}_{l,ref}$. Therefore, the control $\hat{R}_l$ is of the bang-bang-type. The larger the width of the interval $\left[\hat{R}_{l,\min}, \hat{R}_{l,\max}\right]$ is, the larger is the maximum harvested energy. The energy harvested through optimal control may exceed with up to 8% the energy harvested using constant controls. This is in qualitative agreement with results reported in [11] (see their Fig. 3).

When the small reference value $\hat{R}_{l,ref} = 0.004399$ is considered, the control $\hat{R}_l$ is of the bang-bang-type only when the interval $\left[\hat{R}_{l,\min}, \hat{R}_{l,\max}\right]$ is above $\hat{R}_{l,ref}$. In this case, the control jumps between the minimum and maximum allowed values. When the interval $\left[\hat{R}_{l,\min}, \hat{R}_{l,\max}\right]$ is below $\hat{R}_{l,ref}$, the maximum energy is a constant no matter the width of the interval since the optimal control always is the maximum allowed value of $\hat{R}_l$.

In case of the intermediate reference value $\hat{R}_{l,ref} = 0.1$, the maximum energy increases by increasing the width of the interval $\left[\hat{R}_{l,\min}, \hat{R}_{l,\max}\right]$ above the reference value but it depends very little on the interval width if the interval is placed below the reference value.

Further information may be found from Fig. 2. Around the resonance load resistance the optimal solution $\hat{R}_{l,opt}$ is of bang-bang type, with jumps between $\hat{R}_{l,\min}$ and $\hat{R}_{l,\max}$ - see Fig. 2 (a), (c) and the harvested energy increases quite linearly with time – see Fig. 2 (b), (d). Below the resonance load resistance, $\hat{R}_{l,opt} = \hat{R}_{l,\max}$ most of the time except a small number of times from the 15000 moments, when $\hat{R}_{l,opt} = \hat{R}_{l,\min}$, due to the imprecision of the numerical procedure – see Fig. 2 (e), (g), (i), (k) and the harvested energy increases rapidly in the first cycle and has a much slower increase in the next nine cycles – see Fig. 2 (f),(h),(j), (l). The relative energy gain in the first cycle is larger at smaller values of the load resistance (compare Fig. 2 (j), (l) on one hand and Fig. 2 (f), (h) on the other hand.

Bang-bang optimal behavior have been also found in [18] where the dimensionless controls were the parameterized stiffness and the electrical time constant (which incorporate the load resistance) except for some control values due to numerical errors. In that paper the optimal control approach improved the output power by 227% in respect with the case of fixed values of the control parameters. Notice that those fixed values are associated with the optimum of the linear regime.

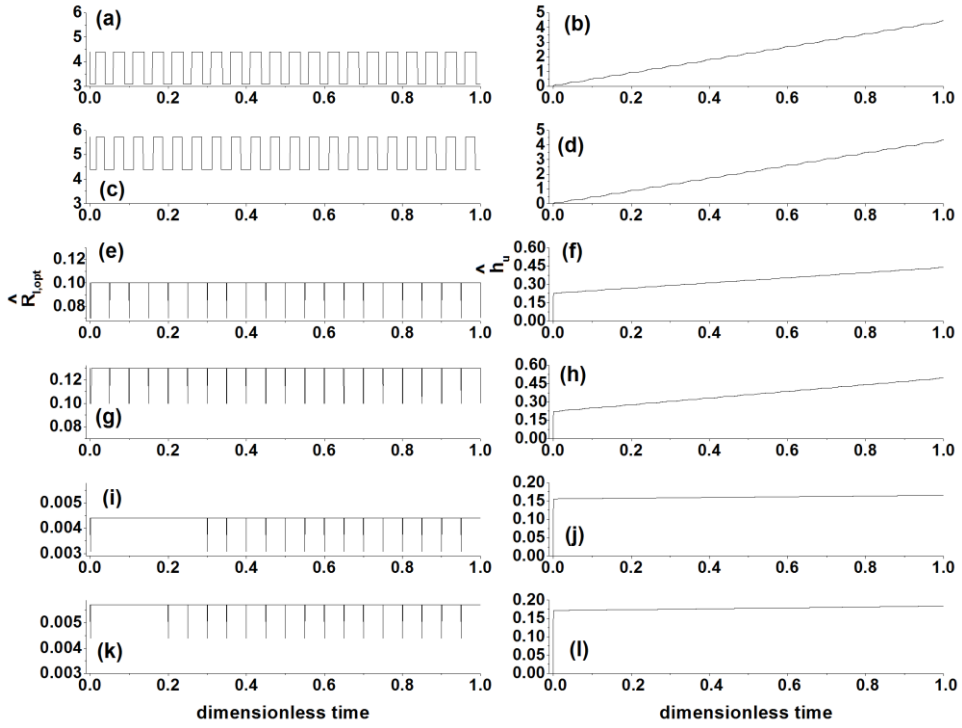

Fig. 2. Optimal control $\hat{R}_{l,opt}$ (left column) and maximum harvested energy $\hat{h}_4$ (right column) as a function of dimensionless time $\hat{\tau}$. (a,b) - $\hat{R}_{l,\min} = 3.519$, $\hat{R}_{l,\max} = 4.399$; (c,d) - $\hat{R}_{l,\min} = 4.399$, $\hat{R}_{l,\max} = 5.718$; (e,f) $\hat{R}_{l,\min} = 0.07$, $\hat{R}_{l,\max} = 0.1$; (g,h) $\hat{R}_{l,\min} = 0.1$, $\hat{R}_{l,\max} = 0.13$; (i,j) $\hat{R}_{l,\min} = 0.003519$, $\hat{R}_{l,\max} = 0.004399$; (k,l) $\hat{R}_{l,\min} = 0.004399$, $\hat{R}_{l,\max} = 0.005718$; Ten cycles are considered ($\hat{\tau}_f = 1$ and $\tau_{ref} = 0.08333\,s$) and $n_{steps} = 15000$.

It is known that the energy harvester response and efficiency is very sensitive to the initial conditions [3]. The performance is usually different in the first cycle as compared with the next ones. The usual approach is to try to obtain a periodic harvester operation. For instance, in [11] the damping electromagnetic coefficient is modulated in such a way that a periodic evolution with the same period as the excitation source is obtained. The objective is to maximize the energy extracted during each period. This is desirable from engineering perspective to have systems evolving with periodic motion of the same period since this allows easier design. Notice that the resonance assumption, which is very often adopted when analyzing the harvester performance on long time intervals, tacitly neglects the influence of

the first cycles [11]. In some cases the harvester may operate for short time intervals and this requires a detailed treatment of the initial phases. Here we shall assume that the harvester operates just one cycle operation. This might be of practical interest for instance when the user needs very small amounts of energy at random moments and switching on the harvester for one cycle ensures the energy need. Therefore, a closer look to the optimal control performance follows in case of harvesting the energy for a single cycle.

Figure 2(f),(h),(j),(l) shows that when the load resistance has relatively small values, a significant amount of energy is harvested in the first cycle. Therefore, the optimization of the system during the first cycle might be of interest for those users who need small enough energy amounts, lower than the energy provided by the system during the first cycle. Several considerations on the optimization of the first cycle follow.

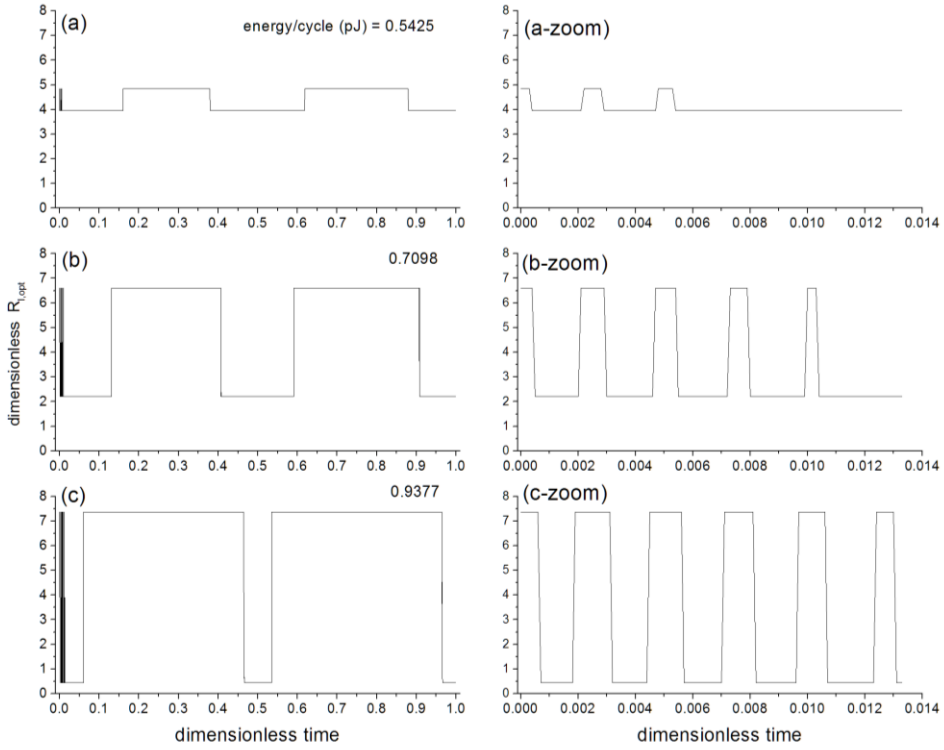

Fig. 3. Dimensionless optimal control $\hat{R}_{l,opt}$ as a function of dimensionless time $\hat{\tau}$. (a) and (a-zoom) - $\hat{R}_{l,min} = 0.9\hat{R}_{ref}$, $\hat{R}_{l,max} = 1.1\hat{R}_{ref}$; (b) and (b-zoom) - $\hat{R}_{l,min} = 0.8\hat{R}_{ref}$, $\hat{R}_{l,max} = 1.2\hat{R}_{ref}$; (c) and (c-zoom) - $\hat{R}_{l,min} = 0.7\hat{R}_{ref}$, $\hat{R}_{l,max} = 1.3\hat{R}_{ref}$; The maximum harvested energy per cycle is also shown. $n_{steps} = 15000$.

Figure 3 shows the time variation of the dimensionless optimal control $\hat{R}_{l,opt}$ around the resonance value $\hat{R}_{ref} = 4.399$. The control is of the bang-bang type, as expected. Extracting a maximum amount of energy from the vibratory system requires a careful control at the beginning of the cycle (see the zoomed figures on the right column). The number of jumps between the minimum and maximum allowed values increases by increasing the width of the interval $\left[\hat{R}_{l,\min}, \hat{R}_{l,\max}\right]$. Also, the maximum harvested energy per cycle increases by increasing the width of that interval.

When the load resistance is significantly smaller than the optimum resonance resistance load, the optimal control is not of bang-bang type but it equals the maximum allowed resistance. This is briefly discussed in the ESM.

Several strategies of controlling the load resistance are presented in Table 5 to harvest the energy of the first cycle. Strategies #1 and #2 assume a constant load resistance, equal with the optimum resonance value or much smaller than it, respectively. Strategies #3 and #4 involve optimal control with the load resistance allowed to vary around the constant values adopted for strategies #1 and #2, respectively.

Table 5. Strategies of controlling the load resistance around the resonance value $R_{l,opt}$ to harvest the energy of the first cycle for the energy sources of Tables 6 and 7.

Operation strategy	Description
#1	R_l = const = $R_{l,opt}$ of Tables 6 and 7
#2	R_l = const = $0.01R_{l,opt}$
#3 (optimal control)	R_l ranges between $0.1R_{l,opt}$ and $1.9R_{l,opt}$
#4 (optimal control)	R_l ranges between $0.001R_{l,opt}$ and $0.019R_{l,opt}$

Details about the implementation of these strategies follow. A common approximation used in literature is the assumption of an infinite internal resistance of the piezoelectric element [17]. The dependence of the results on this assumption is discussed in the ESM. Here a finite value of the piezoelectric element resistance is considered. The accuracy of the results depends on the number of discretization intervals n_{step}. This is shortly discussed in the ESM. The dependence of results on the BOCOP the optimization method is discussed in the ESM. The Midpoint method is recommended and used in the following. The harvested energy depends on the material of the sensor, as expected. This is shortly shown in the ESM. Here the material PZT-5H is used.

The harvester configurations should obey a lower limit on resonance frequency since it increases when the size decreases, as asked by modern network sensors. The frequency usually ranges between 100 and 300 Hz. Comments concerning the dependence of harvester performance on size are shown in ESM. However, size limitation might be surpassed since individual harvesters may be connected in

series or parallel to increase the output or current output. This way the electrical output may be tailored for specific applications [4].

Ambient energy sources are usually not monochromatic but have vibration spectrum which exhibits multiple peaks of significant power For instance, Table 2.2 of [4] shows three acceleration peaks for each energy source. They are: the highest acceleration peak, the highest acceleration peak in the accessible frequency range (i.e. >100 Hz) and a secondary peak in the accessible range. Different peaks may excite different resonance mode of the harvester and this may be followed by strain cancellation and output power decrease. It is desirable to have a tuning mechanism able to control the structure resonance frequency. Here we consider than only the primary vibration mode is excited.

There is still need for further research to estimate the efficiency of power conversion for the various energy harvesters and to establish a minimum vibration level required for positive power generation by these devices. Several sources of energy of smaller and larger acceleration are shown in Tables 6 and 7, respectively. Most of the data correspond to the secondary vibration peak. The acceleration of these sources ranges between 0.000226 and 12 m/s^2. The optimum resonance load resistance $R_{l,opt}$ is also shown in those tables. Generally, energy sources having larger frequency are associated with larger values of output power [4].

Table 6. Sources of energy of smaller acceleration (Table 2.2 of [4].

Index	Energy source	Acceleration a (m/s^2)	Frecquency f (Hz)	Load resistance $R_{l,opt}$ (MOhm)
1	A/C duct: center, low	0.013	113.8	5.456
2	A/C duct: side, high	0.0127	98.8	6.451
3	A/C duct: center, high	0.0186	108.3	5.777
4	Computer side panel	0.036	120	5.127
5	Microwave oven: top	0.57	240	2.368
6	Microwave oven: side	1.276	120	5.127
7	Office desk	0.00516	546.3	0.997
8	Harvard bridge railing	0.0193	136.3	4.422
9	Parking meter: Perp.	0.000697	148.1	4.021
10	Parking meter: Par.	0.000509	977.5	0.549
11	Car hood: 750 rpm	0.0103	510.6	1.065
12	Car hood: 3000 rpm	0.102	880.6	7.424
13	Medium tree	0.000226	240	2.368
14	Small tree	0.000425	99.4	6.407

Table 7. Sources of energy of larger acceleration (Table A3 of [4]).

Index	Energy source	Acceleration a (m/s^2)	Frequency f (Hz)	Load resistance $R_{l,opt}$ (MOhm)
1	Car engine compartment	12	200	2.885
2	Base of 3-axis machine tool	10	70	9.963
3	Blender casing	6.4	121	5.073

4	Clothes dryer	3.5	121	5.073
5	Car instrument panel	3	13	4.671
6	Door frame just after door closes	3	125	4.884
7	Small microwave oven	2.5	121	5.073
8	HVAC vents in office building	1.5	60	12.288
9	Windows next to busy road	0.7	100	6.363
10	CD on notebook computer	0.6	75	9.108
11	Second story floor of busy office	0.2	100	6.363

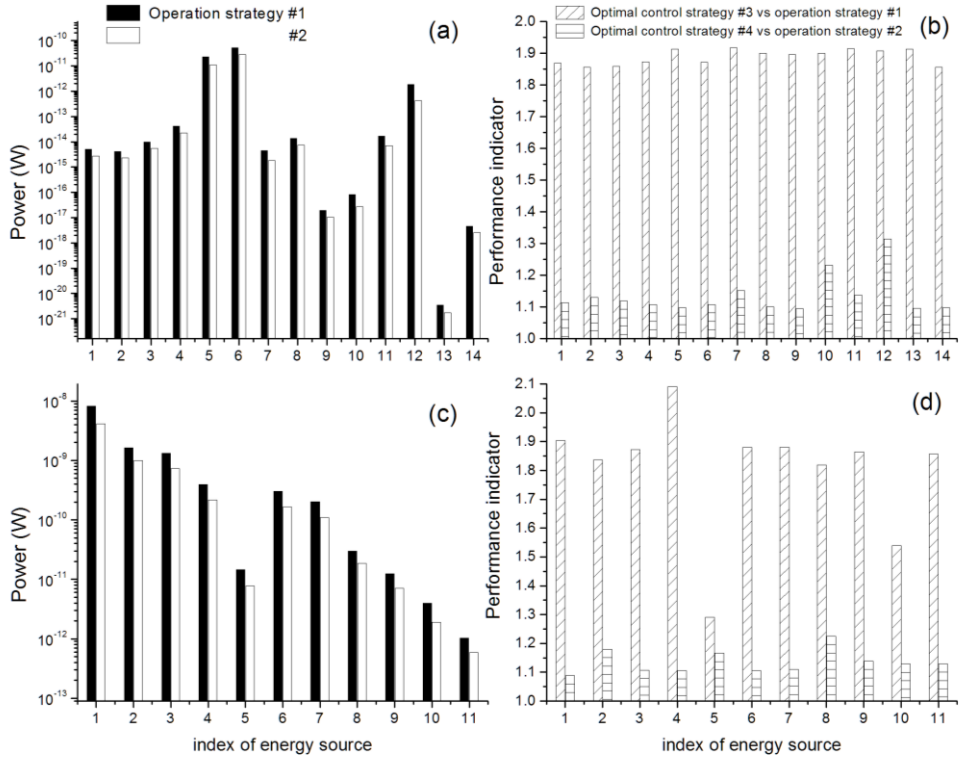

Fig. 4. (a) and (c) – average power per cycle for the energy sources of Tables 6 and 7, respectively. Both strategies #1 and #2 of Table 5 have been considered. (b) and (d) – performance indicator for the optimal control strategies #3 and #4 applied to the energy sources of Tables 6 and 7, respectively.

The strategies #1 and #2 of Table 5 are used as a reference and the following performance indicator is defined to emphasize the improvement of the energy harvesting due to optimal control:

$$\text{Performance indicator} = \frac{P_{3/4}}{P_{1/2}} \tag{14}$$

where $P_{3/4}$ is average power per cycle obtained by optimal control strategy #3 or #4 while $P_{1/2}$ is the average power per cycle obtained by strategy #1 or #2. The power obtained by using the strategies #1 and #2 is shown in Fig. 4(a) for the energy sources of Table 6 and in Fig. 4(c) for those of Table 7. The harvested power ranges between about 10^{-20} and 10^{-8} W.

Strategy #1 provides larger power than strategy #2, as expected. For both strategies, the power obtained increases by increasing the acceleration of the vibratory movement. Using optimal control strategy significantly increases the power when the load resistance is allowed to vary around the optimum resonance value (strategy #3 in Fig. 4(b) and 4(d)). In this case, the performance indicator ranges between about 1.3 and 2.1, depending on the energy source. When the load resistance is much smaller than the optimum resonance value, the optimal control improves in a lesser way the system performance (strategy #4 in Fig. 4(b) and 4(d)). In this case, the performance indicator ranges between about 1.1 and 1.3, depending on the energy source.

A significant issue in case of the energy of a single cycle is harvested is the dependence of the harvested energy on the moment when the optimal control starts. This moment might not coincide with the start of the energy source cycle. Delay aspects are discussed in [20] and in [21] where statistical delay constraints are considered. Delay aspects are shortly treated in ESM. Another issue shortly discussed in the ESM is related with the time dependence of the acceleration of the energy source. Namely, during some cycles that acceleration might have values which are different from its peak value.

3. Conclusions

In case of the resistive load two types of controls are treated: a controllable resistance and a controllable inductance, respectively.

When the controllable resistance is near the resonance value the optimal control is of bang-bang type. The larger is the width $\left[\hat{R}_{l,\min}, \hat{R}_{l,\max}\right]$ of variation of the controllable resistance, the larger is the harvested energy. For values of the controllable resistance smaller than the resonance value, the harvested energy increases by increasing the width of the interval $\left[\hat{R}_{l,\min}, \hat{R}_{l,\max}\right]$ toward the bigger values.

The energy gain in the first cycle is generally larger than in the next cycles. Therefore, the load operation optimization during the first cycle might be of interest for the users who need small enough energy amounts. Several vibratory energy sources are listed in Tables 6 and 7 with acceleration between 0.000226 and 12 m/s^2. Near the resonance resistance the control is of the bang-bang type and a careful control is needed at the beginning of the cycle, when the number of jumps between the minimum and maximum allowed values and the harvested energy increase by increasing the width of the interval $\left[\hat{R}_{l,\min}, \hat{R}_{l,\max}\right]$. The harvested

power for the first cycle ranges between about 10^{-20} and 10^{-8} W. When the load resistance is significantly smaller than the optimum resonance resistance load, the optimal control equals the maximum allowed resistance and the harvested power decreases in comparison with that associated with the resonance resistance.

References

[1] Badescu V., *Best operation strategies for piezoelectric vibration energy harvesters. I. Theory*. Journal of Engineering Sciences and Innovation (JESI), to be published.
[2] Kamali S.H., Moallem M., Arzanpour S., *A self-tuning vibration energy harvester with variable loads and maximum allowable displacement*, Smart Mater. Struct., **27**, 105015, 2018 (8pp).
[3] Hosseinlo A.H., Vu T.L, Turitsyn K., *Optimal control strategies for efficient energy harvesting from ambient vibration*, IEEE 54th Annual conference on decision and control (CDC) December 15-18, Osaka, Japan, 2015, p. 5391-5396.
[4]. Du Toit N.E., *Modeling and design of a MEMS piezoelectric vibration energy harvester*, MsD thesis, MIT, May 2005.
[5] Aleksandrova M.P., Tsanev T.D., Pandiev M., Dobrikov G.H., *Study of piezoelectric behaviour of sputtered $KNbO_3$ nanocoatings for flexible energy harvesting*, Energy, **205**, 2020, p. 118068.
[6] Morangueira Y.L.A., Pereira J.C.C., *Energy harvesting assessment with a coupled full car and piezoelectric model*, Energy, **210**, 2020, p. 118668.
[7]. Renno J.M., Daqaq M.F., Inman D.J., *On the optimal energy harvesting from a vibration source*, J Sound and Vibration, **320**, 2009, p. 386-405.
[8] Badescu V., *Best operation strategies for piezoelectric vibration energy harvesters. III. Application to controllable inductance and capacitive loads*. Journal of Engineering Sciences and Innovation (JESI), to be published
[9] Cassidy I.L., Scruggs J.T., *Statistically linearized optimal control of an electromagnetic vibratory energy harvester*, Smart materials and structures, **21**, 2012, 085003
[10] du Toit N.E., Wardle B.L., *Experimental verification of models for microfabricated piezoelectric vibration energy harvesters*, AIAA Journal, **45**, 2007, p. 1126- 1137.
[11] Caruso G., Galeani S., Menini L., *Optimal semi-active energy harvesting from mechanical oscillator with variable electromechanical damping coefficient: some preliminary properties and numerical results*, 2015 IEEE 54th Annual conference on decision and control (CDC) December 15-18, Osaka, Japan, p. 1966 - 1971
[12] Halvorsen E., *Optimal Load and Stiffness for Displacement-Constrained Vibration Energy Harvesters*, 2016, http: https://arxiv.org/abs/1603.01909
[13] Le C.P., Halvorsen E., *MEMS electrostatic energy harvesters with end-stop effects.* J. Micromech. Microeng, **22**, 2012, 074013 (12pp) doi:10.1088/0960-1317/22/7/074013
[14] Truong B.D., Le C.P., Halvorsen E., *Power optimization and effective stiffness for a vibration energy harvester with displacement constraints*, J. Micromech. Microeng, **26**, 2016, 124006 (8pp)
[15]. Twiefel J., Richter B., Hemsel T., Wallaschek J., *Model based design of piezoelectric energy harvesting systems*, Clark WW, Ahmadian M, Lumsdaine A, editors, Smart Structures and Materials 2006: Damping and Isolation, Proc. SPIE 2006, vol. 6169: 616909
[16]. Mendez V., Campos D., Horsthemke W., *Efficiency of harvesting energy for colored noise by linear oscillators.* Phys. Rev E, **88**, 2013, 022124
[17] Du Toit N.E., Wardle B.L., Kim S.-G., *Design considerations for MEMS-scale piezoelectric mechanical vibration energy harvesters*, Integrated Ferroelectrics: An International Journal, **71**, 2005, p. 121-160.
[18] Le T.T.T., Jost F., Sager S., *Optimal control of vibration-based micro-energy harvesters*. J. Optim Theory Appl, **179**, 2018, p. 1025-1042
[19] Kahaner D.K., Moler C., Nash S., *Numerical Methods and Software*, Prentice Hall, Englewood Clis, 1989.
[20]. Ghouli Z., Hamdi M., Lakrad F., Belhaq M., *Energy harvesting in a nonlinear harvester under modulated delay amplitude*, MEDYNA 2017: 2nd Euro-Mediterranean Conference on Structural

Dynamics and Vibroacoustics, 25-27 April 2017, Sevilla, Spain, http://medyna2017.sciencesconf.org/132565/document

[21] Ahmed I., Phan K.T., Le-Ngoc T., *Optimal stochastic power control for energy harvesting systems with statistical delay constraints*, 2015 IEEE Global Communications Conference (GLOBECOM), San Diego, CA, 2015, p. 1-6, doi: 10.1109/GLOCOM.2015.7417468.